J Pathol Inform

Editor-in-Chief:
Anil V. Parwani , Pittsburgh, PA, USA
Liron Pantanowitz, Pittsburgh, PA, USA

OPEN ACCESS
HTML format

For entire Editorial Board visit : www.jpathinformatics.org/editorialboard.asp

Review Article

Review of advanced imaging techniques

Yu Chen, Chia-Pin Liang, Yang Liu[1], Andrew H. Fischer[2], Anil V. Parwani[3], Liron Pantanowitz[3]

Fischell Department of Bioengineering, University of Maryland, College Park, MD, [1]Medicine and BioEngineering, University of Pittsburgh, Pittsburgh, PA, [2]Pathology, University of Massachusetts, Worcester, MA, [3]Pathology, University of Pittsburgh Medical Center, Pittsburgh, PA, USA

E-mail: *Liron Pantanowitz - pantanowitzl@upmc.edu
*Corresponding author

Received: 12 February 12 Accepted: 28 April 12 Published: 28 May 12

This article may be cited as:
Chen Y, Liang C, Liu Y, Fischer AH, Parwani AV, Pantanowitz L. Review of advanced imaging techniques. J Pathol Inform 2012;3:22.

Available FREE in open access from: http://www.jpathinformatics.org/text.asp?2012/3/1/22/96751

Abstract

Pathology informatics encompasses digital imaging and related applications. Several specialized microscopy techniques have emerged which permit the acquisition of digital images ("optical biopsies") at high resolution. Coupled with fiber-optic and micro-optic components, some of these imaging techniques (e.g., optical coherence tomography) are now integrated with a wide range of imaging devices such as endoscopes, laparoscopes, catheters, and needles that enable imaging inside the body. These advanced imaging modalities have exciting diagnostic potential and introduce new opportunities in pathology. Therefore, it is important that pathology informaticists understand these advanced imaging techniques and the impact they have on pathology. This paper reviews several recently developed microscopic techniques, including diffraction-limited methods (e.g., confocal microscopy, 2-photon microscopy, 4Pi microscopy, and spatially modulated illumination microscopy) and subdiffraction techniques (e.g., photoactivated localization microscopy, stochastic optical reconstruction microscopy, and stimulated emission depletion microscopy). This article serves as a primer for pathology informaticists, highlighting the fundamentals and applications of advanced optical imaging techniques.

Key words: 2-photon microscopy, 4Pi microscopy, advanced imaging, confocal microscopy, digital, microscopy, optical coherence tomography, optics, photoactivated localization microscopy, spatially modulated illumination microscopy, stimulated emission depletion microscopy

Access this article online

Website: www.jpathinformatics.org

DOI: 10.4103/2153-3539.96751

Quick Response Code:

INTRODUCTION

Microscopy is important for diagnostic pathology as well as biomedical informatics research. Transmitted light microscopy has been the main technique for diagnostic pathology for over a century. Recently, several specialized microscopy techniques emerged.[1-4] Table 1 lists several new microscopy modalities and compares them with conventional transmitted light microscopy. These techniques have great potential for clinical diagnostic applications, as they permit imaging to be performed at much higher resolution. Many contemporary instruments not only offer imaging at higher resolution, but allow users to study single molecules and better image live cells. The advent of these new techniques will likely alter the role of pathologists in future diagnoses. Not only may tissue biopsies be replaced by "optical biopsies," but pathologists may be called upon to acquire, manage, and possibly interpret these high resolution digital images. Therefore, a better understanding of these techniques

Table 1: Spectrum of specialized imaging microscopy modalities (adapted in part from reference[120])

Imaging modality	Microscopy principle	Achievable resolution	Pros	Cons
Phase-contrast microscopy	Refractive index differences are used to provide contrast to view unstained microscopic specimens. Small phase shifts in light passing through a transparent specimen get converted into amplitude or contrast changes in the image	Lateral resolution ~200 nm Axial resolution ~500 nm	Can observe living cells/ organisms in a natural/unstained state; can provide more information than specimens that need to be killed, fixed or stained to view under a microscope; high-contrast, high-resolution images	Not ideal for thick organisms or particles; Halo effect, where images are often surrounded by bright areas, might obscure details along the perimeter of the specimen
Fluorescence microscopy (wide-field)	Fluorescence microscopy uses fluorescence instead of transmitted or reflected light	Lateral resolution ~200 nm Axial resolution ~500 nm	Can provide high contrast, high-resolution images; versatile in choosing difference fluorophores and ability to visualize multiple fluorophores simultaneously	Not ideal for thick organisms or particles; needs to stain/process the sample to emit fluorescence; fluorescence signals are usually weak
Confocal microscopy	Confocal microscopy increases optical resolution and contrast. By using a scanning platform where the light source is imaged through a pinhole to block out-of-focus photons, it is possible to reconstruct 3D structures from images	Lateral resolution ~200 nm Axial resolution ~500 nm	Able to provide 3D sectioning by reducing the out-of-focused light; high-resolution images can be acquired rapidly and noninvasively	Relatively high cost and smaller field of view; image depth limited to a few hundreds of microns.
Two-photon microscopy (TPM)	Based on non-linear excitation of fluorophores, this mode of microscopy offers submicron depth-resolved imaging without using a pinhole	Lateral resolution ~300 nm Axial resolution ~900 nm	Wide separation between excitation and emission spectrum ensures rejection of excitation light; deeper image penetration than confocal microscopy, suitable for thick specimens; elimination of confocal pinhole minimizes signal loss	Relatively lower resolution compared to confocal as longer wavelength is used; usually require introducing fluorophores into specimens for imaging
Optical coherence tomography (OCT) and microscopy (OCM)	OCT enables micron scale imaging based on low-coherence interferometry. OCM combines confocal microscopy with OCT to achieve depth-resolved cellular resolution imaging	Lateral resolution ~1000 nm Axial resolution ~900 nm	Can observe living tissues in a natural/unstained state; deeper image penetration than confocal microscopy, suitable for thick specimens; high-speed imaging to image 3D volume *in vivo*	Relatively lower molecular contrast compared to fluorescence imaging
4Pi microscopy	Using two oppositely-aligned objective lenses effectively doubles the angular aperture, permitting greater resolution to be obtained	Lateral resolution ~100 nm Axial resolution ~ 100 nm	Higher resolution than confocal microscopy	Limited resolution improvement compared to STED or PALM/STORM
Structured illumination microscopy (SIM) and saturated SIM (SSIM)	SIM uses laser illumination of samples from which coarse barcode-like interference patterns (Moiré fringes) are emitted and processed to generate high-resolution images	Lateral resolution ~ 100 nm for SIM and ~50 nm for SSIM Axial resolution ~200 nm	Compatible with wide-field microscopy	Limited resolution improvement compared to STED or PALM/STORM; needs data processing
Stimulated emission depletion (STED)	STED uses two beams, one for excitation and the other for quenching. The difference between these two point-spread-functions gives a smaller effective area for excitation	Lateral resolution <10 nm Axial resolution ~30 nm	High resolution; fast for small field of view; no need for data processing	Fluorophore limited.

Table 1 (Contd...)

Table 1 (Contd...)

Imaging modality	Microscopy principle	Achievable resolution	Pros	Cons
Photoactivated localization microscopy (PALM) and stochastic optical reconstruction microscopy (STORM)	PALM and STORM rely on single molecule localization with nanometer accuracy, offering comparable resolution to transmission electron microscopy (TEM)	Lateral resolution ~ 10 nm Axial resolution ~ 10 nm	High resolution; relatively simple setup.	Fluorophore limited; computer-intensive data processing; relatively longer acquisition time
Spatial-domain low-coherence quantitative phase microscopy (SL-QPM)	SL-QPM uses the ultra-high sensitivity of light interference effect to quantify the nanoscale optical path length difference	Lateral resolution ~ 200 nm Axial sensitivity <1 nm	Nanoscale sensitivity to detect the axial structures; use standard clinical histology and cytology slides without modification; can be used in conjunction with conventional pathology	Lateral resolution is still limited by diffraction (>250nm); large data set and computer-intensive signal processing

and their potential uses will be beneficial for the pathology informatics community. This article reviews several advanced microscopy modalities and highlights some of the emerging applications using these optical imaging techniques.

CONFOCAL MICROSCOPY

Confocal microscopy increases optical resolution and contrast. Laser scanning confocal microscopy uses a point light source that is imaged on the sample, with a pinhole placed in front of the detector.[5,6] The use of the pinhole rejects out-of-focus photons from reaching the detector. Confocal microscopy enables the reconstruction of three dimensional (3D) structures by stacking individual 2D *en-face* images at different depths. Microscopy can also be performed with parallel imaging approaches, including slit scanning or tandem scanning.[7] Confocal imaging using dual-axis configuration[8-10] enables imaging at an even deeper penetration.

The scanning laser ophthalmoscope used to examine the retina was the first device utilized for *in vivo* confocal microscopy.[11] Reflectance-mode confocal microscopy (RCM) has also been translated into clinical applications for noninvasive high-resolution imaging of human skin *in vivo*.[12] Confocal laser endomicroscopy (CLE) is a relatively new endoscopic tool that creates high-resolution images of cells and tissues *in vivo*.[13,14] CLE essentially provides *in vivo* histology-level images during ongoing endoscopy. Confocal endomicroscopy can also be performed through fiber bundles[15,16] or a rigid gradient-index (GRIN) rod lens (special rod-shaped optical component that can relay images).[17-19]

TWO-PHOTON MICROSCOPY

Two-photon microscopy (TPM) provides high-resolution (submicron) imaging with lower phototoxicity and deeper tissue penetration than confocal microscopy. In the two-photon process, a molecule simultaneously absorbs two photons whose individual energy is only half of the energy state needed to excite that molecule, and then releases the energy to an emission photon [Figure 1].[20] To achieve reasonable excitation/collection efficiency, typical TPM systems focus the excitation photons into a very tiny volume using a high numerical aperture (NA) objective lens and deliver them in a very short period of time (femtosecond pulse). The first practical TPM system was demonstrated in 1990.[21] TPM uses longer wavelength light for excitation; therefore it can provide deeper penetration depth than single-photon microscopy. Because TPM requires two photons to arrive at the same time and same location to excite the molecule, the fluorescence signal depends on the square of the illumination intensity. Hence, excitation is only appreciable at the focal spot as the illumination intensity rapidly falls off above or below the focal plane. In other words, TPM can perform "optical sectioning" without using the physical pinhole that is used in confocal microscopy. As a result, TPM can collect signals more efficiently than confocal microscopy.[22,23]

TPM can image conventional fluorophores or fluorescent proteins such as green fluorescent protein (GFP). It can also image endogenous fluorescence molecules such as the reduced nicotinamide adenine dinucleotide (NADH), flavin adenine dinucleotide (FAD), and keratin, among others.[24] In addition, second harmonic generation (SHG), an energy-conserving scattering process which also absorbs two incident photons at once and release all the energy to the emission photon (at the half of the wavelength of the incident photons), can provide direct visualization of anisotropic biological structures such as collagen.[24] Intravital TPM has provided unprecedented anatomical, cellular, molecular, and functional insights into host-tumor interactions[25] as well as immune cell dynamics.[26,27] Such dynamic intravital microscopy is transformative as it can reveal cellular behavior *in vivo*.[28] It was recently demonstrated that TPM can also excite fluorescence

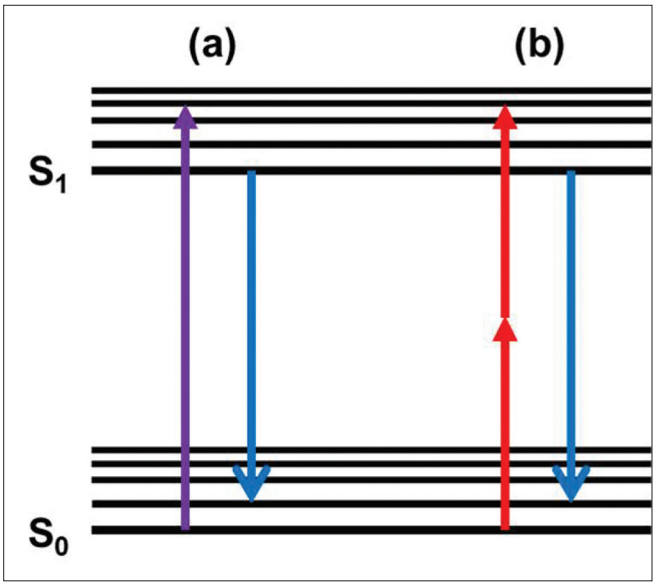

Figure 1: Jablonski diagram for single photon (a) and two-photon (b) excitation

directly from hemoglobin,[29,30] allowing investigators to directly visualize microvasculature. The rich biological information provided by TPM therefore makes it an attractive tool for biomedical imaging applications.

Traditional TPM image formation uses 2D raster scanning (line-by-line scanning), which could be slow for applications requiring high temporal resolution. Hence, other imaging approaches have been developed, including random-access scanning using acousto-optic deflectors (AODs), a device that can change beam deflection angle by tuning the input electric frequency applied on the acoustic crystal,[31] and parallel scanning with multiple beams.[32] More recently, alternative scanningless TPM using temporal focusing has been developed.[33] Instead of allowing laser pulse traveling through the optical system with constant pulse duration, temporal focusing broadens the pulse duration along with the propagation path, and reaches the shortest pulse duration only at the focal plane of the objective. This approach, also called plane-projection multiphoton microscopy, enables video-rate wide-field optical sectioning of live tissues.[34] Rapid 3D imaging of living cells has been achieved using novel Bessel beam plane illumination microscopy.[35] Bessel beam has a relatively long focusing waist compared to a conventional Gaussian beam. Coupled with structural illumination and/or two-photon excitation, this method provides isotropic (in all directions) resolution of 0.3 μm and rapid imaging speed of 200 planes per second, thereby enabling 3D imaging of subcellular features *in vivo*. With this technology the dynamics of mitochondria, filopodia, membrane ruffles, intracellular vesicles, and mitotic chromosomes in living cells have accordingly been visualized in real-time.[35] Figure 2 shows an example of Bessel plane two-photon excitation imaging of chromosomes during mitosis.[35]

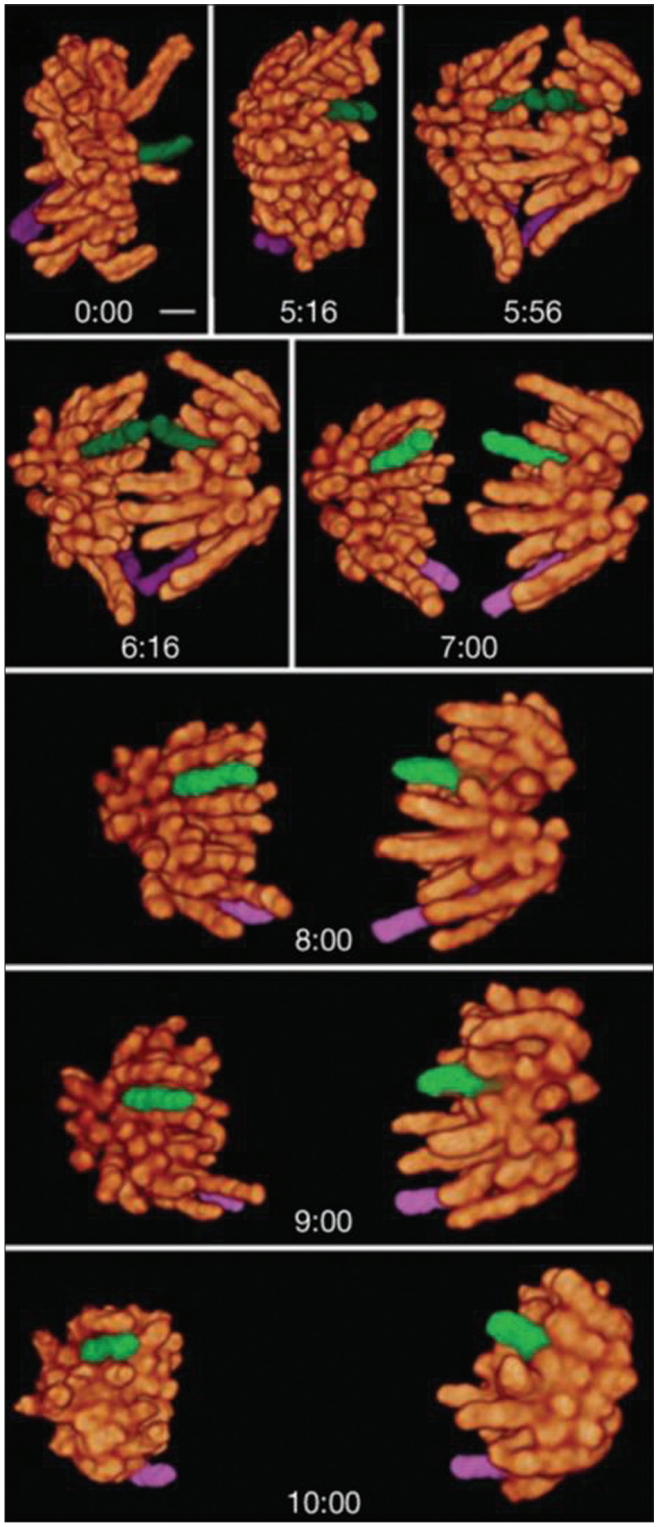

Figure 2: High-speed volumetric imaging of chromosomes in mitosis using scanned Bessel beams in conjunction with two-photon excitation. The images shown demonstrate 3D tracing of two chromatids (green and purple) in a living cell over a series of eight image planes. (Reproduced with permission from reference 35.)

Typical TPM systems use an excitation wavelength at ~800 nm. To further improve the penetration depth of TPM, longer wavelength excitation at ~1300 nm can be

used.[36] To further extend TPM imaging for subsurface tissues, several two-photon microendoscopes using GRIN rod lens or fiber bundles have been developed.[17,37-39] In those designs, the GRIN rod lens or fiber bundles relays the light from the proximal end of the endoscope to the distal end (in the tissue). Alternatively, Wu *et al*, developed a 2.4-mm-in-diameter all-fiber-optic endomicroscopy using a piezoelectric transducer (PZT) scanner (a device that can deform its shape based on the applied voltage) at the distal tip.[40,41] Two-photon microendoscopy enables numerous applications such as imaging neuronal function and the gastrointestinal or reproductive tract.[3]

OPTICAL COHERENCE TOMOGRAPHY AND MICROSCOPY

Optical coherence tomography (OCT) is analogous to ultrasound imaging, except that the imaging is performed using light rather than sound.[42-44] By measuring the echo time delay and intensity of back-reflected light, OCT can reveal tissue microstructure with micron-level resolution and 1-2 mm penetration depth, approaching those of standard excisional biopsy and histopathology, but without the need of tissue removal.[45-47] Since the speed of light is much faster than that of sound, the echo delay time in OCT is detected using a technique called low coherence interferometry.[48-50] Figure 3 shows a schematic diagram of a Michelson interferometer. OCT uses a broad bandwidth light source; therefore interference signal is only observed when the path lengths of the reference and sample arms are matched to within the coherence length (the length over which the phase of optic wave oscillation is correlated) of the light. By scanning the reference mirror position, the magnitude and echo time delay (equivalent to depth) of the reflected light from the sample can be measured. The optical beam can be scanned across the tissue surface to form 2D or 3D images. The contrast in OCT comes from the difference in light scattering properties in various tissue layers, and as a result, OCT can reveal tissue microstructure without the use of contrast agents (i.e., label-free imaging).

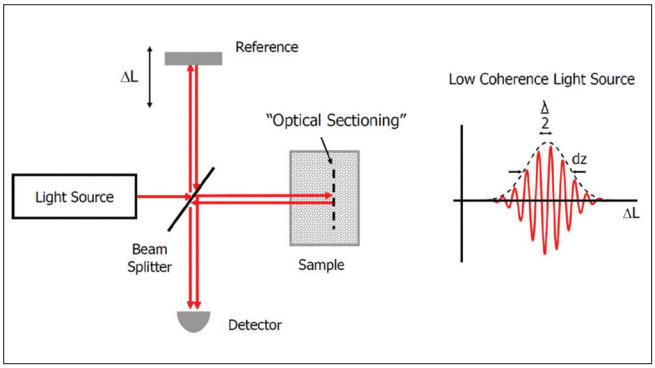

Figure 3: Schematic diagram of an OCT system using a Michelson interferometer

The axial resolution of OCT is determined by the coherence length of the light source: Dz = (2ln2/pi (pi=3.14159)) (l^2/Dl), where Dl is the full-width-at-half-maximum of the source spectrum (the difference between the two wavelength values at which the power is equal to half of its maximum value) and l is the center wavelength of the source spectrum.[51] From this equation, broadband light sources can achieve high axial resolution. Typical OCT systems can achieve axial resolutions of ~10-15 μm. More sophisticated broadband light sources can generate a broadband spectrum and hence result in ultrahigh-resolution OCT imaging.[52,53] The transverse resolution of OCT is the same as that in optical microscopy, and is determined by the diffraction limit of the focused optical beam: Dx = (4l/pi (pi=3.14159))(f/d), where d is the beam size on the objective lens and f is its focal length (the distance from the lens to the focus spot). Fine transverse resolution can be obtained by using a large numerical aperture (NA) objective that focuses the beam on a small spot size. The combination of a very broad bandwidth light source and Bessel beam[54-56] has culminated in the realization of micro-OCT with 1-2 μm isotropic resolution in 3D.[57]

Optical coherence microscopy (OCM) combines confocal microscopy with OCT to achieve cellular resolution imaging in the en-face plane (the plane parallel to the surface of the sample).[58-64] The combination of coherence and confocal gates enhances rejection of unwanted scattered light, thereby allowing improved imaging depth compared to confocal microscopy alone. Figure 4 shows representative OCM images of human colon specimens *ex vivo*.[65] Representative histology images in this figure at the corresponding depth in this figure show good correlation with the OCM images. Detailed structures such as crypt lumens and translucent mucin-containing cells can be clearly visualized. Also shown in this figure is the 3D isosurface view of two central colonic crypts. Various types of organs have been shown to be amenable to *ex vivo* study using full-field OCT.[66] As high-resolution OCT images are able to recapitulate the main histological features in tissues, this technique looks promising in performing fast histology, especially in intraoperative procedures. In addition, OCM has been demonstrated to provide high-resolution images of renal pathology in real time without exogenous contrast medium or histological processing. High sensitivity and specificity was achieved using OCM to differentiate normal from neoplastic renal tissues, suggesting possible applications for guiding renal mass biopsies or evaluating surgical margins.[67]

Using fiber-optic and micro-optic components, OCT can be integrated with a wide range of imaging devices such as endoscopes, laparoscopes, catheters, and needles to enable imaging inside the body.[47,68-75] Endomicroscopic

OCT provides unique advantages for evaluating diseases present within the epithelial surface of hollow organs as well as buried in deep solid organs. Clinical applications of endoscopic OCT/OCM include the detection of pre-malignant lesions, identification of disease below the tissue surface, assessment of depth of tumor invasion, localization of cancer margins, evaluation of effectiveness of therapy, and reduction in the number of biopsies and frequency of surveillance.[69,76-78] Figure 5 shows an example of a forward-viewing OCT imaging needle that can be used for neurosurgery guidance. The OCT image obtained can clearly identify anatomic landmarks that can be used in stereotactic surgery.[79] Simultaneous OCT and Doppler OCT (DOCT) imaging is also possible. DOCT measures the frequency shift of the back-scattered photons caused by the motion of samples (e.g., red blood cells). This technique has been used to quantify the blood flow velocity in biological samples.[78]

The development of endoscopic OCT greatly facilitates imaging of certain conditions. For example, OCT has been shown to be successful at detecting intestinal metaplasia in patients with Barrett's esophagus patients[80-84] and transmural inflammation in those who have inflammatory bowel disease.[85] OCT also has the potential to distinguish hyperplastic from adenomatous polyps in the colon.[86] Of particular interest, is the fact that OCT may be useful in identifying high-grade dysplasia, such as in Barrett's esophagus. However, additional work in this area is still required. Evans *et al*. reported a sensitivity of 83% and specificity of 75% for detecting high-grade dysplasia and intramucosal carcinoma with blinded scoring of OCT images from 55 patients.[87] Isenberg *et al*. reported a sensitivity of 68% and a specificity of 82%, with an accuracy of 78% for the detection of dysplasia in biopsies from 33 patients with Barrett's esophagus.[88] Employing computer-aided diagnosis, Qi *et al*. found an increased sensitivity of 82%, a specificity of 74%, and an accuracy of 83% in 13 patients.[89] It is anticipated that further improvements in spatial resolution will hopefully result in better diagnostic capability.

OCT/OCM can perform high-resolution imaging of tissue structures *in situ* and in real time. Images are available immediately without the need for excision and histological processing of a specimen. The development of high-resolution and high-speed OCT technology, as well as OCT endoscopic devices, will soon provide clinicians with more diagnostically relevant information in increasing clinical applications. Potential applications of OCT/OCM in pathology might include enhanced specimen grossing, reduced need for frozen sections during intraoperative consultation,[90] and direct scanning of tissue blocks to produce 3D histology images, potentially bypassing certain steps involving glass slide workflow.[91]

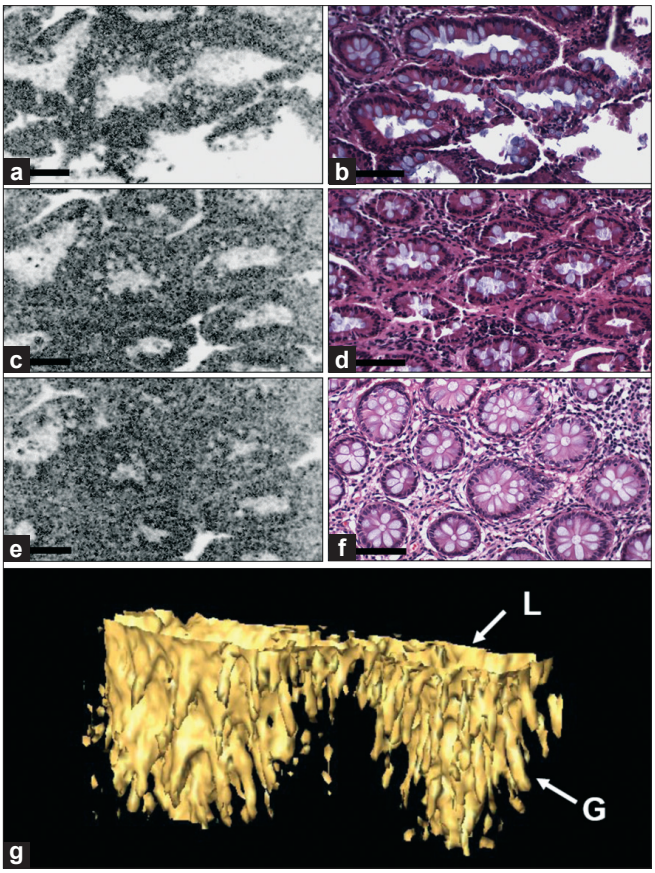

Figure 4: Line-scanning OCM images (a,c,e) and corresponding histology (b,d,f) at different depths: 40 mm (a,b); 100 mm (c,d); 150 mm (e,f). Bar = 100 m. (g) 3D isosurface view of two central crypts, including their lumens (l) and the adjacent goblet cells (g). 3D object size is 360 mm ´ 170 mm × 145 mm (depth). (Reproduced with permission from reference 65)

SUPER-RESOLUTION MICROSCOPY

Super-resolution microscopy refers to a suite of techniques that pushes or breaks the diffraction limit (~200-300 nm in the lateral direction and ~500-700 nm in the axial direction) to achieve a spatial resolution down to ~8-25 nm,[4,92] thereby allowing the observation of subcellular structures that are not visible in conventional light microscopy. One category of methods overcomes the diffraction limit by using patterned excitation to sharpen the point spread function (PSF) of the imaging system, including saturated structured illumination microscopy (SSIM)[93] and stimulated emission depletion (STED) microscopy.[94] The other category uses single molecule localization techniques (i.e., statistically sample the point source to locate the center of the Airy disk) to accurately identify the object position, such as photoactivated localization microscopy (PALM),[95] fluorescence photoactivated localization microscopy (FPALM),[96] and stochastic optical reconstruction microscopy (STORM).[97]

Structured illumination microscopy (SIM) illuminates the sample using a sinusoidally modulated stripe pattern with

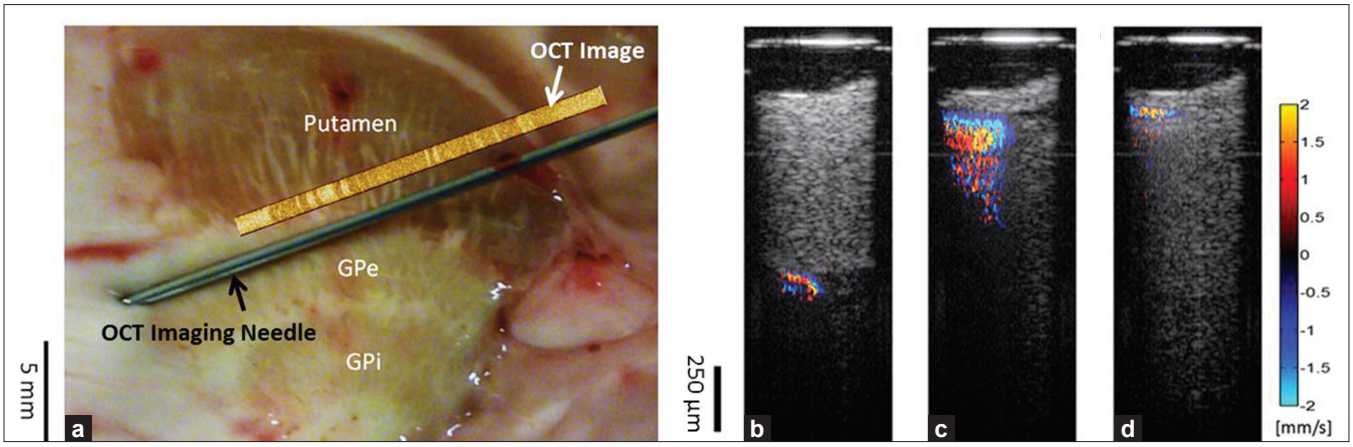

Figure 5: (a) A 21-gauge needle OCT probe overlying the human basal ganglia (PUT = putamen, GPe= globus pallidus externa, GPi = globus pallidus interna). Above it is the full-track reconstructed expanded OCT image that was created *ex vivo*. (b-d) Simultaneous OCT and Doppler OCT (DOCT) imaging of an anesthetized sheep brain *in vivo* showing real-time monitoring of vessel compression by the OCT probe. (Reproduced with permission from reference 79)

a spatial frequency (i.e., how often the sinusoidal structure repeats per unit of distance). Each spatial frequency from the sample interferes with this illumination frequency, resulting in a coarse beat frequency (moiré fringes), which can be resolved by a conventional microscope Hence, structured illumination increases the highest detectable spatial frequency, or equivalently, increases the spatial resolution of conventional optical microscopy. SIM extends the resolution by a factor of 2 (~100 nm).[98] Saturated SIM can generate harmonics with spatial frequencies that are multiples of modulation frequency.[93] Less than 50 nm resolution has been demonstrated using SSIM.[93] SIM can also be extended to generate 3D views [Figure 6] by mixing three beams.[99,100] 3D SIM images demonstrate much improved lateral and axial resolution over conventional wide-field microscopy. Since SIM uses wide-field illumination, it can achieve a high imaging speed for live cell imaging *in vivo*. Recently, video imaging at 11 Hz with 100 nm resolution has been demonstrated.[101]

In contrast, STED overcomes the diffraction limit by employing stimulated emission to "turn off" the fluorophores in the focal region, except those located at the center.[94,102] In STED, two beams are used, one as in conventional fluorescence microscopy to excite the fluorophores from the ground state to the excited state [Figure 7a] and the other beam (STED beam) to stimulate the excited state to spontaneously revert back to the ground state (a process called stimulated emission) where no fluorescence photon is emitted. By making the STED beam a "donut" shape using a phase mask [Figure 7b], much smaller PSF can be achieved [Figure 7c]. STED can provide an xy resolution of ~30 nm.[4] The axial resolution initially attained was ~100 nm with a single lens,[103] and can be improved to ~30-40 nm when using 4Pi geometry.[104] STED exhibits 10-fold higher resolution (20-30 nm) to visualize biological structures more clearly. Furthermore, by applying pulsed excitation together with time-gated detection (where the detection event is triggered by the excitation pulse), sharper images with 35% enhancement in resolution can be obtained at 2-3 times lower average power.[105]

Another category of super-resolution microscopy relies on single (or sparse) molecule localization, where the localization of the fluorophore can be estimated by statistically sampling to find the center of the fuzzy Airy disk.[106] The accuracy of single molecule localization can reach nanometer accuracy[92] despite the broad PSF (>200 nm). PALM[95] and FPALM[96] use photoactivatable fluorescence proteins (FAP, FPs that can be turned on and off by a UV laser, for example EosGFP.[107]). Initially, the fluorophores are in an inactive state (nonfluorescence). When shinning with a flash of UV light, the dye is photoactivated into a fluorescing state. Since the photoactivation process is stochastic, only a few, well-separated molecules are "turned on" at a given time. The position of those molecules can be located by single molecule localization techniques described above. After those fluorophores photobleach, another flash of light is applied to activate another random set of fluorophores. This process is repeated many times, and the final image is the summation of the individual images. Because the image is built up molecule by molecule at different times, the final image resolution can be much higher than the diffraction limit. PALM is hence able to visualize detailed mitochondria structures with comparable resolution as TEM. Furthermore, dual-color PALM enables direct visualization of molecular interactions at the nanometer level (resolution ~20 nm).[108] One limitation of the single molecule localization technique is the long data acquisition time (several hours). However, a recent form of PALM decreased the acquisition time to ~25 s per frame with 60 nm resolution,[109] therefore allowing live-cell PALM imaging of nanoscale adhesion dynamics. Recently, Pavani *et al*. used an engineered PSF to form

a double helix pattern in 3D, whose angular orientation rotates with the axial (z) position of the emitter.[110] Each z position was associated with a unique orientation of two spots that could be resolved by a diffraction limited detector, thereby allowing precise single molecule localization in 3D.[110,111] This method can be used for traditional wide-field fluorescence microscopy, as well as super-resolution microscopy such as PALM.

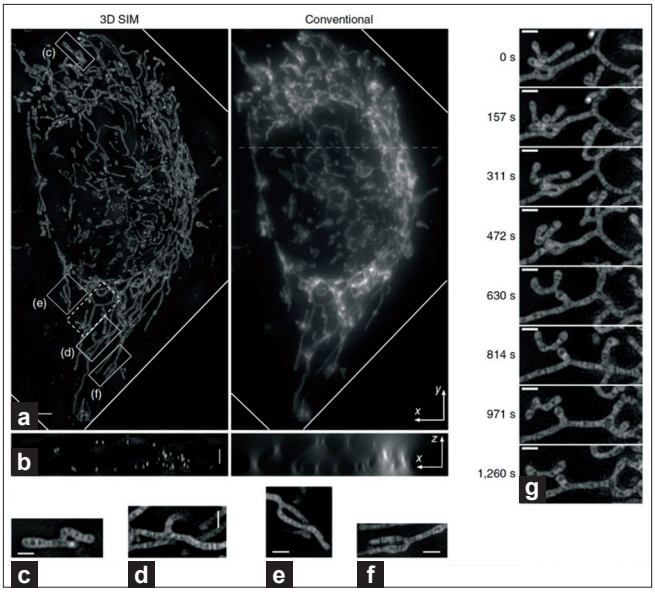

Figure 6: Live 3D SIM and conventional wide-field microscopy images showing the mitochondria dynamics in living HeLa cells. (a) Maximum-intensity projection along z dimension through the cell. (b) One x–z cross-section of the same volume sliced through the dashed line shown in a. (c–f) Single-plane x–y slices corresponding to the boxed regions in a. (g) Eight time frames of the region boxed with a dashed line in (a). Each frame is a maximum-intensity projection along z over a 1.3 m thickness that contains the featured 'Y'-shaped mitochondrion. Scale bars are 2 μm (a,b) and 1 μm (c–g). (Reproduced with permission from reference 100.)

Another localization-based technique called STORM uses a pair of different organic dyes (called the "activator" and "reporter") at close proximity (a few nanometers) to achieve photoswitching,[97,112] and forms super-resolution images using a similar algorithm to that used in PALM. The reporter is often a cyanine dye (Cy5, Cy5.5, or Cy7), and the activator is usually a shorter wavelength cyanine dye (Cy2 or Cy3). The advantage is that different combinations of dye pairs can be simultaneously imaged. Recently, the Zhuang group extended high-resolution STORM to an axial dimension with ~50 nm resolution by using a cylindrical lens.[113] The depth (z) information can be inferred by the ellipticity of the measured PSF. Live-cell 3D STORM imaging [Figure 8] with ~30 nm lateral resolution, ~50 nm axial resolution and 1-2 second temporal resolution (with several independent snapshots) has been achieved.[114] In Figure 8 STORM images clearly discriminate transferrin and clathrin, which appeared as completely overlapping puncta in the conventional images. As demonstrated in this image, the morphology of the clathrin coat enclosing the transferrin cluster was resolved in this nanoscopic cellular structure.[114]

SPATIAL-DOMAIN LOW-COHERENCE QUANTITATIVE PHASE MICROSCOPY

Spatial-domain low-coherence quantitative phase microscopy (SL-QPM) is a novel optical microscopy technique based on the light interference effect (i.e., superimposition of a reference wave and a sample wave), developed to detect subtle changes in cell architecture as small as 0.9 nm, a scale much smaller than the resolution of a light microscope.[115-118] SL-QPM quantifies optical refractive index distribution by physical parameter of optical path length (OPL), associated with the macromolecular density or organization within a

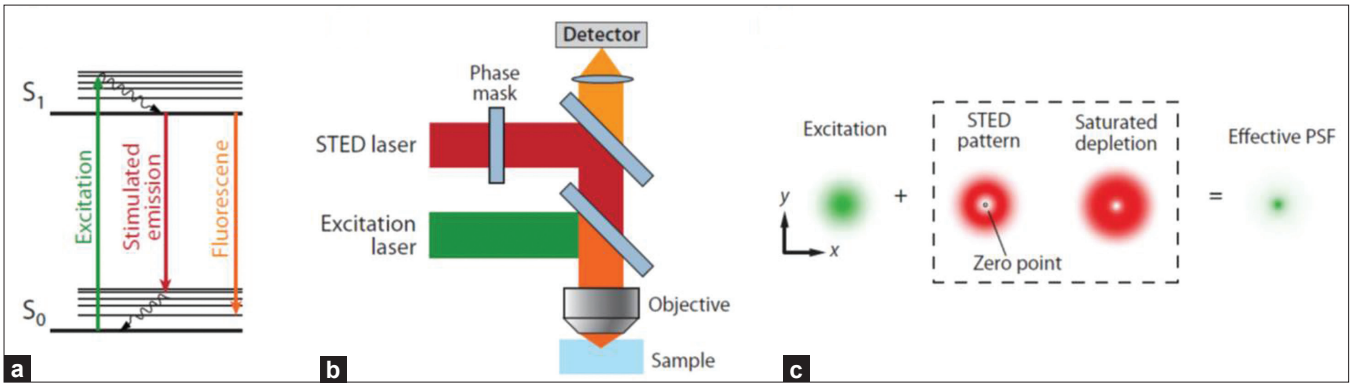

Figure 7: (a) The process of stimulated emission. A ground state (S0) fluorophore can absorb a photon from excitation light and jump to the excited state (S1). Spontaneous fluorescence emission brings the fluorophore back to the ground state. Stimulated emission happens when the excited-state fluorophore encounters another photon with a wavelength comparable to the energy difference between the ground and excited state. (b) Schematic drawing of a STED microscope. The excitation laser and STED laser are combined and focused into the sample through the objective. A phase mask is placed in the light path of the STED laser to create a specific pattern at the objective focal point. (c) In the xy mode, a donut-shaped STED laser is applied with the zero point overlapped with the maximum of the excitation laser focus. With saturated depletion, fluorescence from regions near the zero point is suppressed, leading to a decreased size of the effective PSF. (Reproduced with permission from reference 4.)

single cell or a subcellular component (e.g., nucleus). Importantly, this technique is suitable for analyzing the nanoscale structural changes of cell nuclei in original, unmodified cytology and histology specimens prepared using standard clinical protocols, without any additional processing or modification.

The instrument used to perform SL-QPM is shown in Figure 9. Briefly, parallel white light is focused onto the sample by a low-NA objective. The reflectance-mode signals are projected by a lens onto the slit of a spectrograph coupled with a charge couple device (CCD) camera, which is mounted on a scanning stage. The detected backscattering spectrum is the result of superimposition of the reference wave (i.e., reflection from the glass) and backscattered sample waves with a shared common light path. Due to the intrinsic variation of stain levels, a correction model has also been developed to minimize the effect of stain-induced variations on the measured OPL.[119] The nanoscale-sensitive architectural parameters provide a comprehensive quantitative assessment of nuclear structural characteristics. For example, the average OPL of the cell nucleus is associated with the average nuclear density;[115] while the intranuclear standard deviation of OPL or entropy[117] quantifies the chromatin texture of the cell nucleus.

The SL-QPM system has shown great potential for improving the detection of malignancy even in cells morphologically labeled as "normal" or "indeterminate" by expert surgical pathologists and/or cytopathologists that were confirmed at surgery to be malignant;[117] or in histologically "normal" appearing cells from uninvolved tissue distant from the primary cancer site.[116] Figure 10 shows an example of analyzing the original unmodified histology specimens of breast biopsies processed with a standard clinical protocol (formalin fixed, paraffin embedded and stained with hematoxylin and eosin) using the SL-QPM system. Figure 10a shows the representative histology image and the corresponding OPL map of cell nuclei from three groups of cells, including "normal" cells from patients undergoing a reduction mammoplasty, "uninvolved" cells (i.e., histologically normal cells located at a distance from a nearby malignant tumor), and "malignant" cells. The average OPL from the cell nuclei in this figure shows a progressive increase in normal, uninvolved and malignant cells. More importantly, although both normal and uninvolved cells both appear to be morphologically "normal" by histopathological diagnosis with a light microscope, the average nuclear OPL is significantly elevated in the uninvolved cells of the cancer specimen when compared to normal cells from the reduction mammoplasty.

CONCLUSION

Advanced microscopy techniques have shown great promise for imaging biological structures at the cellular, subcellular and molecular level. These tools have increasingly enabled the visualization of cellular and molecular interactions *in situ* at the submicron to nanometer scale, thereby furthering our understanding of the fundamental biological and pathological mechanisms involved in many diseases. With further development in technology, these microscopy techniques will likely provide novel tools beyond what is currently available in the arsenal of pathologists. It is important that pathologists therefore understand these advanced imaging techniques and the impact they have on pathology.

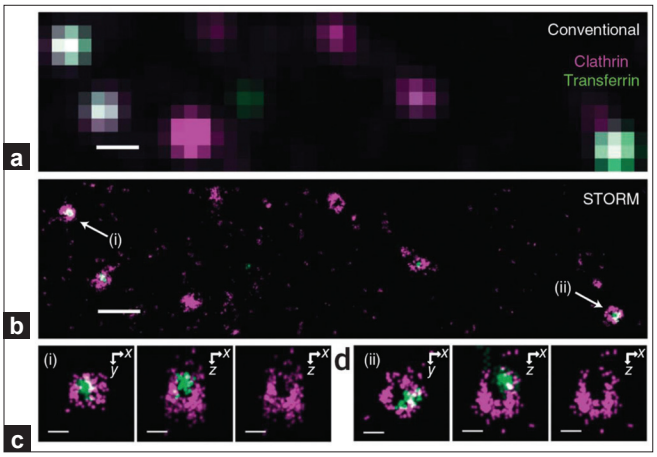

Figure 8: An example of two-color 3D STORM images of transferrin and clathrin in live cells. (a) Conventional image of clathrin coated pits (CCPs) and transferrin in a live cell. (b) A 3D STORM image x-y projection of the same area taken in 30 seconds. (c,d) STORM images of CCPs indicated in b: x-y cross-section near the plasma membrane (left), x-z cross-section cutting through the middle of the invaginating CCP (middle) and corresponding x-z cross-section of the clathrin channel only (right). Scale bars are 500 nm (a,b) and 100 nm (c,d). (Reproduced with permission from reference 114.)

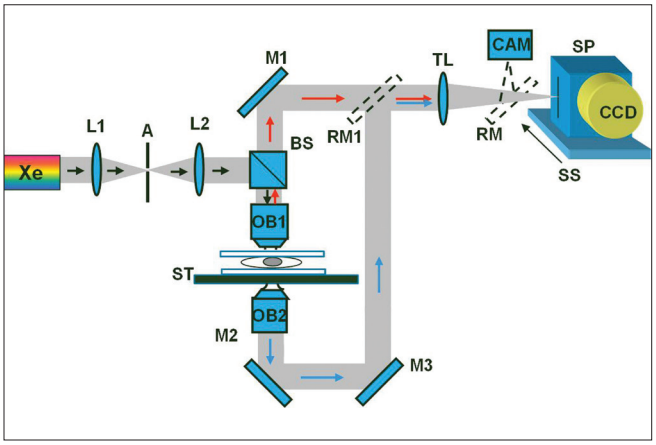

Figure 9: The SL-QPM system. (Xe: Xenon-arc lamp; L: lens; A: aperture; BS: beam splitter; OB: objective; ST: sample stage; M: mirror; RM: removal mirror; TL; tube lens; CAM: camera; SP: spectrograph; SS: scanning stage; CCD: charged coupled device (CCD) camera.)

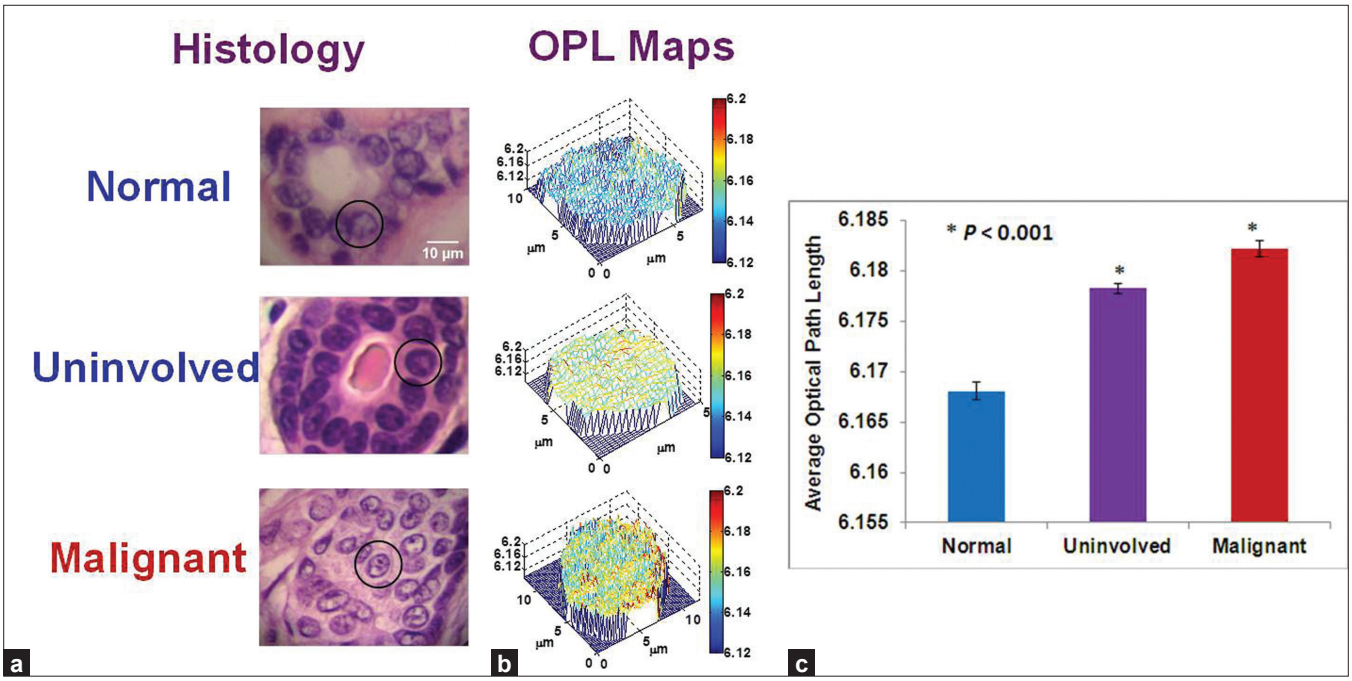

Figure 10: (a) Representative histology images of breast tissue and (b) the corresponding optical path length (OPL) maps of cell nuclei are shown from normal, uninvolved (i.e., histologically normal cells adjacent to tumor) and malignant cells. (c) By analyzing approximately 30-40 cell nuclei per group, the average optical path length of normal, uninvolved and malignant cell nuclei are significantly increased, when compared to the normal cell nuclei (*t*-test, two-sided *P*-value < 0.001)

REFERENCES

1. Davis I. The 'super-resolution' revolution. Biochem Soc Trans 2009;37:1042-4.
2. Van de Water L. Specialized imaging techniques. Clin Lab Med 1997;17:299-314.
3. Schmolze DB, Standley C, Fogarty KE, Fischer AH. Advances in microscopy techniques. Arch Pathol Lab Med 2011;135:255-63.
4. Huang B, Bates M, Zhuang X. Super-resolution fluorescence microscopy. Annu Rev Biochem 2009;78:993-1016.
5. Rajadhyaksha M, Gonzalez S, Zavislan JM, Anderson RR, Webb RH. *In vivo* confocal scanning laser microscopy of human skin II: advances in instrumentation and comparison with histology. J Invest Dermatol 1999;113:293-303.
6. Rajadhyaksha M, Grossman M, Esterowitz D, Webb RH, Anderson RR. *In vivo* confocal scanning laser microscopy of human skin: melanin provides strong contrast. J Invest Dermatol 1995;104:946-52.
7. Tanbakuchi AA, Rouse AR, Gmitro AF. Monte Carlo characterization of parallelized fluorescence confocal systems imaging in turbid media. J Biomed Opt 2009;14:044024.
8. Wang TD, Mandella MJ, Contag CH, Kino GS. Dual-axis confocal microscope for high-resolution *in vivo* imaging. Opt Lett 2003;28:414-6.
9. Wang TD, Contag CH, Mandella MJ, Chan NY, Kino GS. Confocal fluorescence microscope with dual-axis architecture and biaxial postobjective scanning. J Biomed Opt 2004;9:735-42.
10. Wong LK, Mandella MJ, Kino GS, Wang TD. Improved rejection of multiply scattered photons in confocal microscopy using dual-axes architecture. Opt Lett 2007;32:1674-6.
11. Webb RH, Hughes GW, Delori FC. Confocal scanning laser ophthalmoscope. Appl Opt 1987;26:1492-9.
12. Nori S, Rius-Diaz F, Cuevas J, Goldgeier M, Jaen P, Torres A, *et al.* Sensitivity and specificity of reflectance-mode confocal microscopy for *in vivo* diagnosis of basal cell carcinoma: a multicenter study. J Am Acad Dermatol 2004;51:923-30.
13. Kiesslich R, Burg J, Vieth M, Gnaendiger J, Enders M, Delaney P, *et al.* Confocal laser endoscopy for diagnosing intraepithelial neoplasias and colorectal cancer *in vivo*. Gastroenterology 2004;127:706-13.
14. Paull PE, Hyatt BJ, Wassef W, Fischer AH. Confocal laser endomicroscopy: a primer for pathologists. Arch Pathol Lab Med 2011;135:1343-8.
15. Gmitro AF, Aziz D. Confocal microscopy through a fiber-optic imaging bundle. Opt Lett 1993;18:565.
16. Hsiung PL, Hardy J, Friedland S, Soetikno R, Du CB, Wu AP, *et al.* Detection of colonic dysplasia *in vivo* using a targeted heptapeptide and confocal microendoscopy. Nat Med 2008;14:454-8.
17. Kim P, Puoris'haag M, Cote D, Lin CP, Yun SH. *In vivo* confocal and multiphoton microendoscopy. J Biomed Opt 2008;13:010501.
18. Chen CW, Blackwell TR, Naphas R, Winnard PT Jr, Raman V, Glunde K, *et al.* Development of Needle-Based Microendoscopy for Fluorescence Molecular Imaging of Breast Tumors Models. J Innov Opt Health Sci 2009;2:343-52.
19. Pillai RS, Lorenser D, Sampson DD. Deep-tissue access with confocal fluorescence microendoscopy through hypodermic needles. Opt Express 2011;19:7213-21.
20. Goeppert-Mayer M. Über elementarakte mit zwei quantensprüngen. Ann Phys 1931;3:273-94.
21. Denk W, Strickler JH, Webb WW. Two-photon laser scanning fluorescence microscopy. Science 1990;248:73-6.
22. So PT, Dong CY, Masters BR, Berland KM. Two-photon excitation fluorescence microscopy. Annu Rev Biomed Eng 2000;2:399-429.
23. Zipfel WR, Williams RM, Webb WW. Nonlinear magic: multiphoton microscopy in the biosciences. Nat Biotechnol 2003;21:1369-77.
24. Zipfel WR, Williams RM, Christie R, Nikitin AY, Hyman BT, Webb WW. Live tissue intrinsic emission microscopy using multiphoton-excited native fluorescence and second harmonic generation. Proc Natl Acad Sci U S A 2003;100:7075-80.
25. Jain RK, Munn LL, Fukumura D. Dissecting tumour pathophysiology using intravital microscopy. Nat Rev Cancer 2002;2:266-76.
26. Steven P, Bock F, Huttmann G, Cursiefen C. Intravital two-photon microscopy of immune cell dynamics in corneal lymphatic vessels. PLoS One 2011;6:e26253.
27. Victora GD, Schwickert TA, Fooksman DR, Kamphorst AO, Meyer-Hermann M, Dustin ML, *et al.* Germinal center dynamics revealed by multiphoton microscopy with a photoactivatable fluorescent reporter. Cell 2010;143:592-605.

28. Sakadzic S, Roussakis E, Yaseen MA, Mandeville ET, Srinivasan VJ, Arai K, *et al*. Two-photon high-resolution measurement of partial pressure of oxygen in cerebral vasculature and tissue. Nat Methods 2010;7:755-9.
29. Zheng W, Li D, Zeng Y, Luo Y, Qu JY. Two-photon excited hemoglobin fluorescence. Biomed Opt Express 2010;2:71-9.
30. Li D, Zheng W, Zeng Y, Luo Y, Qu JY. Two-photon excited hemoglobin fluorescence provides contrast mechanism for label-free imaging of microvasculature *in vivo*. Opt Lett 2011;36:834-6.
31. Salome R, Kremer Y, Dieudonne S, Leger JF, Krichevsky O, Wyart C, *et al*. Ultrafast random-access scanning in two-photon microscopy using acousto-optic deflectors. J Neurosci Methods 2006;154:161-74.
32. Kim KH, Buehler C, Bahlmann K, Ragan T, Lee WC, Nedivi E, *et al*. Multifocal multiphoton microscopy based on multianode photomultiplier tubes. Opt Express 2007;15:11658-78.
33. Oron D, Tal E, Silberberg Y. Scanningless depth-resolved microscopy. Opt Express 2005;13:1468-76.
34. Yu JY, Kuo CH, Holland DB, Chen Y, Ouyang M, Blake GA, *et al*. Wide-field optical sectioning for live-tissue imaging by plane-projection multiphoton microscopy. J Biomed Opt 2011;16:116009.
35. Planchon TA, Gao L, Milkie DE, Davidson MW, Galbraith JA, Galbraith CG, *et al*. Rapid three-dimensional isotropic imaging of living cells using Bessel beam plane illumination. Nat Methods 2011;8:417-23.
36. Kobat D, Durst ME, Nishimura N, Wong AW, Schaffer CB, Xu C. Deep tissue multiphoton microscopy using longer wavelength excitation. Opt Express 2009;17:13354-64.
37. Jung JC, Schnitzer MJ. Multiphoton endoscopy. Opt Lett 2003;28:902-4.
38. Levene MJ, Dombeck DA, Kasischke KA, Molloy RP, Webb WW. *In vivo* multiphoton microscopy of deep brain tissue. J Neurophysiol 2004;91:1908-12.
39. Gobel W, Kerr JN, Nimmerjahn A, Helmchen F. Miniaturized two-photon microscope based on a flexible coherent fiber bundle and a gradient-index lens objective. Opt Lett 2004;29:2521-3.
40. Wu Y, Leng Y, Xi J, Li X. Scanning all-fiber-optic endomicroscopy system for 3D nonlinear optical imaging of biological tissues. Opt Express 2009;17:7907-15.
41. Wu Y, Xi J, Cobb MJ, Li X. Scanning fiber-optic nonlinear endomicroscopy with miniature aspherical compound lens and multimode fiber collector. Opt Lett 2009;34:953-5.
42. Huang D, Swanson EA, Lin CP, Schuman JS, Stinson WG, Chang W, *et al*. Optical coherence tomography. Science 1991;254:1178-81.
43. Fujimoto JG, Pitris C, Boppart SA, Brezinski ME. Optical coherence tomography: an emerging technology for biomedical imaging and optical biopsy. Neoplasia 2000;2:9-25.
44. Fujimoto JG. Optical coherence tomography for ultrahigh resolution *in vivo* imaging. Nat Biotechnol 2003;21:1361-7.
45. Fujimoto JG, Brezinski ME, Tearney GJ, Boppart SA, Bouma B, Hee MR, *et al*. Optical biopsy and imaging using optical coherence tomography. Nat Med 1995;1:970-2.
46. Brezinski ME, Tearney GJ, Bouma BE, Izatt JA, Hee MR, Swanson EA, *et al*. Optical coherence tomography for optical biopsy. Properties and demonstration of vascular pathology. Circulation 1996;93:1206-13.
47. Tearney GJ, Brezinski ME, Bouma BE, Boppart SA, Pitris C, Southern JF, *et al*. *In vivo* endoscopic optical biopsy with optical coherence tomography. Science 1997;276:2037-9.
48. Gilgen HH, Novak RP, Salathe RP, Hodel W, Beaud P. Submillimeter optical reflectometry. IEEE Journal of Lightwave Technology 1989;7:1225-33.
49. Takada K, Yokohama I, Chida K, Noda J. New measurement system for fault location in optical waveguide devices based on an interferometric technique. Appl Opt 1987;26:1603-6.
50. Youngquist RC, Carr S, Davies DE. Optical coherence-domain reflectometry: a new optical evaluation technique. Optics Letters 1987;12:158-60.
51. Swanson EA, Huang D, Hee MR, Fujimoto JG, Lin CP, Puliafito CA. High-speed optical coherence domain reflectometry. Opt Lett 1992;17:151-3.
52. Drexler W, Morgner U, Kartner FX, Pitris C, Boppart SA, Li XD, *et al*. *In vivo* ultrahigh-resolution optical coherence tomography. Opt Lett 1999;24:1221-3.
53. Unterhuber A, Povazay B, Bizheva K, Hermann B, Sattmann H, Stingl A, *et al*. Advances in broad bandwidth light sources for ultrahigh resolution optical coherence tomography. Phys Med Biol 2004;49:1235-46.
54. Ding Z, Ren H, Zhao Y, Nelson JS, Chen Z. High-resolution optical coherence tomography over a large depth range with an axicon lens. Opt Lett 2002;27:243-5.
55. Leitgeb RA, Villiger M, Bachmann AH, Steinmann L, Lasser T. Extended focus depth for Fourier domain optical coherence microscopy. Opt Lett 2006;31:2450-2.
56. Lee KS, Rolland JP. Bessel beam spectral-domain high-resolution optical coherence tomography with micro-optic axicon providing extended focusing range. Opt Lett 2008;33:1696-8.
57. Liu L, Gardecki JA, Nadkarni SK, Toussaint JD, Yagi Y, Bouma BE, *et al*. Imaging the subcellular structure of human coronary atherosclerosis using micro-optical coherence tomography. Nat Med 2011;17:1010-4.
58. Izatt JA, Hee MR, Owen GM, Swanson EA, Fujimoto JG. Optical coherence microscopy in scattering media. Opt Lett 1994;19:590-2.
59. Izatt JA, Kulkarni MD, Wang HW, Kobayashi K, Sivak MV Jr. Optical coherence tomography and microscopy in gastrointestinal tissues. IEEE J Sel Top Quantum Electron 1996;2:1017-28.
60. Aguirre AD, Hsiung P, Ko TH, Hartl I, Fujimoto JG. High-resolution optical coherence microscopy for high-speed, *in vivo* cellular imaging. Opt Lett 2003;28:2064-6.
61. Huang SW, Aguirre AD, Huber RA, Adler DC, Fujimoto JG. Swept source optical coherence microscopy using a Fourier domain mode-locked laser. Opt Express 2007;15:6210-7.
62. Aguirre AD, Chen Y, Bryan B, Mashimo H, Huang Q, Connolly JL, *et al*. Cellular resolution *ex vivo* imaging of gastrointestinal tissues with optical coherence microscopy. J Biomed Opt 2010;15:016025.
63. Chen Y, Huang SW, Aguirre AD, Fujimoto JG. High-resolution line-scanning optical coherence microscopy. Opt Lett 2007;32:1971-3.
64. Dubois A, Grieve K, Moneron G, Lecaque R, Vabre L, Boccara C. Ultrahigh-resolution full-field optical coherence tomography. Appl Opt 2004;43:2874-83.
65. Chen Y, Huang SW, Zhou C, Potsaid B, Fujimoto JG. Improved Detection Sensitivity of Line-Scanning Optical Coherence Microscopy. IEEE J Sel Top Quantum Electron in press;
66. Jain M, Shukla N, Manzoor M, Nadolny S, Mukherjee S. Modified full-field optical coherence tomography: A novel tool for rapid histology of tissues. J Pathol Inform 2011;2:28.
67. Lee HC, Zhou C, Cohen DW, Mondelblatt AE, Wang Y, Aguirre AD, *et al*. Integrated optical coherence tomography and optical coherence microscopy imaging of ex vivo human renal tissues. J Urol 2012;187:691-9.
68. Xie T, Xie H, Fedder GK, Pan Y. Endoscopic optical coherence tomography with a modified microelectromechanical systems mirror for detection of bladder cancers. Appl Opt 2003;42:6422-6.
69. Yaqoob Z, Wu J, McDowell EJ, Heng X, Yang C. Methods and application areas of endoscopic optical coherence tomography. J Biomed Opt 2006;11:063001.
70. Sergeev A, Gelikonov V, Gelikonov G, Feldchtein F, Kuranov R, Gladkova N, *et al*. *In vivo* endoscopic OCT imaging of precancer and cancer states of human mucosa. Opt Express 1997;1:432-40.
71. Tran PH, Mukai DS, Brenner M, Chen Z. *In vivo* endoscopic optical coherence tomography by use of a rotational microelectromechanical system probe. Opt Lett 2004;29:1236-8.
72. Li X, Chudoba C, Ko T, Pitris C, Fujimoto JG. Imaging needle for optical coherence tomography. Opt Lett 2000;25:1520-2.
73. Han S, Sarunic MV, Wu J, Humayun M, Yang C. Handheld forward-imaging needle endoscope for ophthalmic optical coherence tomography inspection. J Biomed Opt 2008;13:020505.
74. Tsai TH, Potsaid B, Kraus MF, Zhou C, Tao YK, Hornegger J, *et al*. Piezoelectric-transducer-based miniature catheter for ultrahigh-speed endoscopic optical coherence tomography. Biomed Opt Express 2011;2:2438-48.
75. Lorenser D, Yang X, Kirk RW, Quirk BC, McLaughlin RA, Sampson DD. Ultrathin side-viewing needle probe for optical coherence tomography. Opt Lett 2011;36:3894-6.
76. Suter MJ, Vakoc BJ, Yachimski PS, Shishkov M, Lauwers GY, Mino-Kenudson M, *et al*. Comprehensive microscopy of the esophagus in human patients with optical frequency domain imaging. Gastrointest Endosc 2008;68:745-53.
77. Chen Y, Aguirre AD, Hsiung PL, Desai S, Herz PR, Pedrosa M, *et al*. Ultrahigh resolution optical coherence tomography of Barrett's esophagus: preliminary descriptive clinical study correlating images with histology. Endoscopy 2007;39:599-605.

78. Yang VX, Tang SJ, Gordon ML, Qi B, Gardiner G, Cirocco M, *et al*. Endoscopic Doppler optical coherence tomography in the human GI tract: initial experience. Gastrointest Endosc 2005;61:879-90.
79. Liang CP, Wierwille J, Moreira T, Schwartzbauer G, Jafri MS, Tang CM, *et al*. A forward-imaging needle-type OCT probe for image guided stereotactic procedures. Opt Express 2011;19:26283-94.
80. Bouma BE, Tearney GJ, Compton CC, Nishioka NS. High-resolution imaging of the human esophagus and stomach *in vivo* using optical coherence tomography. Gastrointest Endosc 2000;51:467-74.
81. Sivak MV Jr, Kobayashi K, Izatt JA, Rollins AM, Ung-Runyawee R, Chak A, *et al*. High-resolution endoscopic imaging of the GI tract using optical coherence tomography. Gastrointest Endosc 2000;51:474-9.
82. Li XD, Boppart SA, Van Dam J, Mashimo H, Mutinga M, Drexler W, *et al*. Optical coherence tomography: advanced technology for the endoscopic imaging of Barrett's esophagus. Endoscopy 2000;32:921-30.
83. Poneros JM, Brand S, Bouma BE, Tearney GJ, Compton CC, Nishioka NS. Diagnosis of specialized intestinal metaplasia by optical coherence tomography. Gastroenterology 2001;120:7-12.
84. Evans JA, Bouma BE, Bressner J, Shishkov M, Lauwers GY, Mino-Kenudson M, *et al*. Identifying intestinal metaplasia at the squamocolumnar junction by using optical coherence tomography. Gastrointest Endosc 2007;65:50-6.
85. Shen B, Zuccaro G Jr, Gramlich TL, Gladkova N, Trolli P, Kareta M, *et al*. *In vivo* colonoscopic optical coherence tomography for transmural inflammation in inflammatory bowel disease. Clin Gastroenterol Hepatol 2004;2:1080-7.
86. Pfau PR, Sivak MV Jr, Chak A, Kinnard M, Wong RC, Isenberg GA, *et al*. Criteria for the diagnosis of dysplasia by endoscopic optical coherence tomography. Gastrointest Endosc 2003;58:196-202.
87. Evans JA, Poneros JM, Bouma BE, Bressner J, Halpern EF, Shishkov M, *et al*. Optical coherence tomography to identify intramucosal carcinoma and high-grade dysplasia in Barrett's esophagus. Clin Gastroenterol Hepatol 2006;4:38-43.
88. Isenberg G, Sivak MV Jr, Chak A, Wong RC, Willis JE, Wolf B, *et al*. Accuracy of endoscopic optical coherence tomography in the detection of dysplasia in Barrett's esophagus: a prospective, double-blinded study. Gastrointest Endosc 2005;62:825-31.
89. Qi X, Sivak MV, Isenberg G, Willis JE, Rollins AM. Computer-aided diagnosis of dysplasia in Barrett's esophagus using endoscopic optical coherence tomography. J Biomed Opt 2006;11:044010.
90. Fine JL. Comment on "Modified full-field optical coherence tomography: A novel tool for rapid histology of fresh tissues". J Pathol Inform 2011;2:29.
91. Fine JL, Kagemann L, Wollstein G, Ishikawa H, Schuman JS. Direct scanning of pathology specimens using spectral domain optical coherence tomography: a pilot study. Ophthalmic Surg Lasers Imaging 2010;41 Suppl:S58-64.
92. Toprak E, Kural C, Selvin PR. Super-accuracy and super-resolution getting around the diffraction limit. Methods Enzymol 2010;475:1-26.
93. Gustafsson MG. Nonlinear structured-illumination microscopy: wide-field fluorescence imaging with theoretically unlimited resolution. Proc Natl Acad Sci U S A 2005;102:13081-6.
94. Hell SW, Wichmann J. Breaking the diffraction resolution limit by stimulated emission: stimulated-emission-depletion fluorescence microscopy. Opt Lett 1994;19:780-2.
95. Betzig E, Patterson GH, Sougrat R, Lindwasser OW, Olenych S, Bonifacino JS, *et al*. Imaging intracellular fluorescent proteins at nanometer resolution. Science 2006;313:1642-5.
96. Hess ST, Girirajan TP, Mason MD. Ultra-high resolution imaging by fluorescence photoactivation localization microscopy. Biophys J 2006;91:4258-72.
97. Bates M, Huang B, Dempsey GT, Zhuang X. Multicolor super-resolution imaging with photo-switchable fluorescent probes. Science 2007;317:1749-53.
98. Gustafsson MG. Surpassing the lateral resolution limit by a factor of two using structured illumination microscopy. J Microsc 2000;198:82-7.
99. Gustafsson MG, Shao L, Carlton PM, Wang CJ, Golubovskaya IN, Cande WZ, *et al*. Three-dimensional resolution doubling in wide-field fluorescence microscopy by structured illumination. Biophys J 2008;94:4957-70.
100. Shao L, Kner P, Rego EH, Gustafsson MG. Super-resolution 3D microscopy of live whole cells using structured illumination. Nat Methods 2011;8:1044-6.
101. Kner P, Chhun BB, Griffis ER, Winoto L, Gustafsson MG. Super-resolution video microscopy of live cells by structured illumination. Nat Methods 2009;6:339-42.
102. Hell SW, Kroug M. Ground-state-depletion fluorescence microscopy - a concept for breaking the diffraction resolution limit. Applied Physics B-Lasers and Optics 1995;60:495-7.
103. Klar TA, Jakobs S, Dyba M, Egner A, Hell SW. Fluorescence microscopy with diffraction resolution barrier broken by stimulated emission. Proc Natl Acad Sci U S A 2000;97:8206-10.
104. Dyba M, Hell SW. Focal spots of size lambda/23 open up far-field fluorescence microscopy at 33 nm axial resolution. Phys Rev Lett 2002;88:163901.
105. Vicidomini G, Moneron G, Han KY, Westphal V, Ta H, Reuss M, *et al*. Sharper low-power STED nanoscopy by time gating. Nat Methods 2011;8:571-3.
106. Thompson RE, Larson DR, Webb WW. Precise nanometer localization analysis for individual fluorescent probes. Biophys J 2002;82:2775-83.
107. Wiedenmann J, Ivanchenko S, Oswald F, Schmitt F, Rocker C, Salih A, *et al*. EosFP, a fluorescent marker protein with UV-inducible green-to-red fluorescence conversion. Proc Natl Acad Sci U S A 2004;101:15905-10.
108. Shroff H, Galbraith CG, Galbraith JA, White H, Gillette J, Olenych S, *et al*. Dual-color superresolution imaging of genetically expressed probes within individual adhesion complexes. Proc Natl Acad Sci U S A 2007;104:20308-13.
109. Shroff H, Galbraith CG, Galbraith JA, Betzig E. Live-cell photoactivated localization microscopy of nanoscale adhesion dynamics. Nat Methods 2008;5:417-23.
110. Pavani SR, Thompson MA, Biteen JS, Lord SJ, Liu N, Twieg RJ, *et al*. Three-dimensional, single-molecule fluorescence imaging beyond the diffraction limit by using a double-helix point spread function. Proc Natl Acad Sci U S A 2009;106:2995-9.
111. Thompson MA, Biteen JS, Lord SJ, Conley NR, Moerner WE. Molecules and methods for super-resolution imaging. Methods Enzymol 2010;475:27-59.
112. Bates M, Huang B, Zhuang X. Super-resolution microscopy by nanoscale localization of photo-switchable fluorescent probes. Curr Opin Chem Biol 2008;12:505-14.
113. Huang B, Wang W, Bates M, Zhuang X. Three-dimensional super-resolution imaging by stochastic optical reconstruction microscopy. Science 2008;319:810-3.
114. Jones SA, Shim SH, He J, Zhuang X. Fast, three-dimensional super-resolution imaging of live cells. Nat Methods 2011;8:499-508.
115. Bista RK, Uttam S, Wang P, Staton K, Choi S, Bakkenist CJ, *et al*. Quantification of nanoscale nuclear refractive index changes during the cell cycle. J Biomed Opt 2011;16:070503.
116. Wang P, Bista R, Bhargava R, Brand RE, Liu Y. Spatial-domain low-coherence quantitative phase microscopy for cancer diagnosis. Opt Lett 2010;35:2840-2.
117. Wang P, Bista RK, Khalbuss WE, Qiu W, Uttam S, Staton K, *et al*. Nanoscale nuclear architecture for cancer diagnosis beyond pathology via spatial-domain low-coherence quantitative phase microscopy. J Biomed Opt 2010;15:066028.
118. Wang P, Bista RK, Qiu W, Khalbuss WE, Zhang L, Brand RE, *et al*. An insight into statistical refractive index properties of cell internal structure via low-coherence statistical amplitude microscopy. Opt Express 2010;18:21950-8.
119. Uttam S, Bista RK, Hartman DJ, Brand RE, Liu Y. Correction of stain variations in nuclear refractive index of clinical histology specimens. J Biomed Opt 2011;16:116013.
120. Toomre D, Bewersdorf J. A new wave of cellular imaging. Annu Rev Cell Dev Biol 2010;26:285-314.